CHALMERS

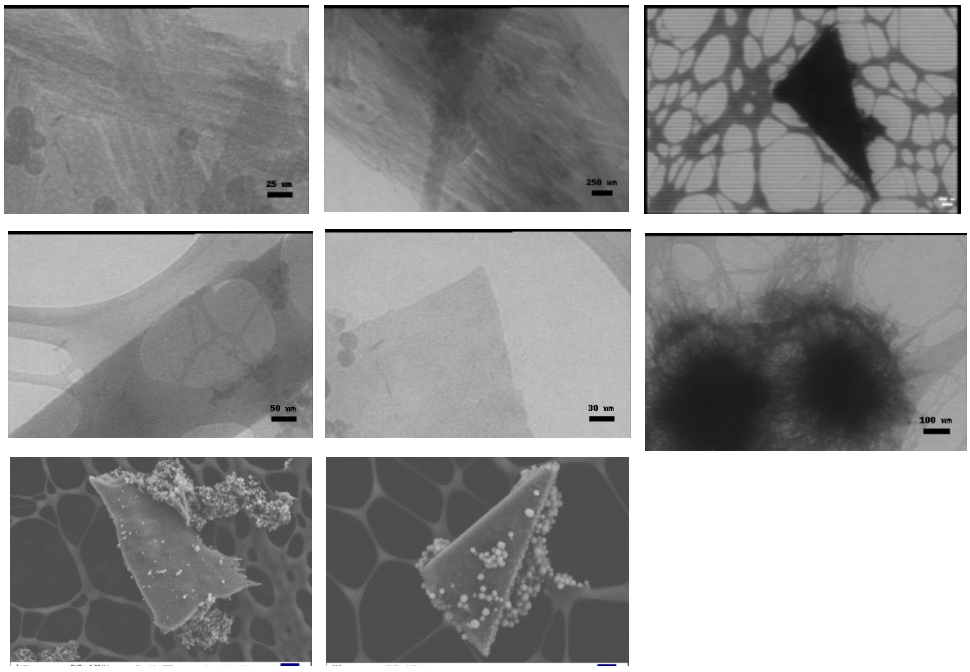

Controllable Calcium Phosphate Morphogenesis Utilizing Surfactant Self-assembly

Master of Science Thesis [The Materials Chemistry and Nanotechnology Program]

Yu Fu

Department of Chemical and Biological Engineering
Division of Applied Surface Chemistry
CHALMERS UNIVERSITY OF TECHNOLOGY
Gothenburg, Sweden, 2012

THESIS FOR DEGREE OF MASTER OF SCIENCE

Controllable Calcium Phosphate Morphogenesis Utilizing Surfactant Self-assembly

Yu Fu

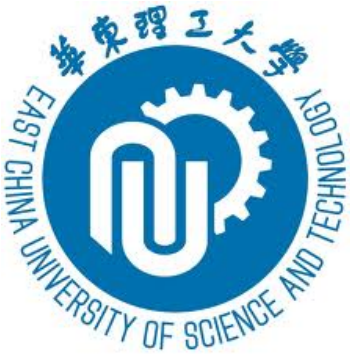

Supervised by Wenxiao He
Professor: Martin Andersson

Department of Chemical and Biological Engineering
Chalmers University of Technology

Gothenburg, Sweden 2012.

Controllable Calcium Phosphate Morphogenesis Utilizing Surfactant Self-assembly

Department of Chemical and Biological Engineering
Chalmers University of Technology
SE-41296 Gothenburg
Sweden
Telephone+46(0)31-772 1000

Cover:
First two rows: TEM images of various nanostructured calcium phosphates.
The last row: SEM images of nanostructured calcium phosphate meso-crystals.
By adjusting the reaction conditions, calcium phosphates with different structures can be formed.

Gothenburg, Sweden, 2012

Controllable calcium phosphate morphogenesis utilizing surfactant self-assembly

Yu Fu
Applied surface chemistry
Department of chemical and biological engineering
Chalmers University of Technology

Abstract:

One major constituent in skeletal tissues, such as bone and teeth, is calcium phosphate (CaP) mineral. In bone, the mineral growth, final composition, and morphology of CaPs are modulated by organic biomacromolecules, such as collagen, in the extracellular matrix.

In this project, liquid crystalline phases (LCPs) formed by surfactant self-assembly were utilized as templates to mimic the collagen matrix in bone, for the study of CaP morphogenesis. CaP formation in LCP templates with different structures was explored, including lamellar phase (L_α), normal hexagonal phase (H_1), bicontinuous cubic phase (I_1), and reverse hexagonal phase (H_2). Two different reaction strategies were investigated, namely beaker method and petri dish method.

The morphology of the obtained CaP particles was primarily examined by Transmission Electron Microscopy (TEM) and Scanning Electron Microscopy (SEM). CaP rods with diameters in the range of 6–20 nm and sheets with widths of ~250 nm and thickness of a few nanometers were successfully obtained from H_2 and L_α LCPs. Moreover, faceted particles with micrometer dimensions were formed from H_1 and I_1 templates.

Keywords: Amorphous calcium phosphate (ACP), Liquid crystalline phase (LCP), Pluronic L64, F127, Calcium phosphate (CaP) morphogenesis.

Contents

1 Introduction

1.1 Calcium phosphate (CaP)

There are three kinds of CaPs; ortho- (PO_4^{3-}), pyro- ($P_2O_7^{4-}$) and poly- ($(PO_3)_n^{n-}$) phosphate [1]. Here we just discuss about calcium orthophosphate. Table 1 shows some common polymorphs of calcium orthophosphate [2]. Among these CaPs, dicalcium phosphate dehydrate (brushite) and dicalcium phosphate anhydrate (monetite) are widely used as dicalcium phosphate cements. Hydroxyapatite (HA) has long been used in bone regeneration since HA bears a large resemblance to bone mineral. It has already been intensively applied in bioceramic coatings of metallic implants and bone fillers to fill bone defects, etc.

Table 1: common forms of calcium phosphates [1]

Ca/P ratio	**Compound**	**Formula**
0.5	Monocalcium phosphate monohydrate (MCPM)	$Ca(H_2PO_4)\bullet H_2O$
0.5	Monocalcium phosphate anhydrate (MCPA)	$Ca(H_2PO_4)_2$
1.0	Dicalcium phosphate dehydrate (DCPD, brushite)	$CaHPO_4\bullet 2H_2O$
1.0	Dicalcium phosphate anhydrate (DCPA, monetite)	$CaHPO_4$
1.33	Octacalcium phosphate (OCP)	$Ca_8(HPO_4)_2(PO_4)_4\bullet 5H_2O$
1.5	α-Tricalcium phosphate (α-TCP)	$\alpha\text{-}Ca_3(PO_4)_2$
1.5	β-Tricalcium phosphate (β-TCP)	$\beta\text{-}Ca_3(PO_4)_2$
1.2-2.2	Amorphous calcium phosphate (ACP)	$Ca_x(PO4)_y\bullet nH_2O$
1.67	Hydroxyapatite (HA)	$Ca_{10}(PO_4)_6(OH)_2$
2.0	Tetracalcium phosphate (TTCP)	$Ca_4(PO_4)O$

1.2 Amorphous calcium phosphate (ACP)

ACP is a class of calcium orthophosphate salts with Ca/P ratio in the range of 1.2–2.2 [1]. ACP has marvelous physicochemical properties, which contribute to its promising role in tissue engineering. Specifically: 1. ACP can easily transform into crystalline phase with the existence of H_2O [1]; 2. ACP can trigger biomineralization as it is firstly forms in matrix vesicles [1]; 3. ACP bears large resemblance with the mineral in calcified mammalian tissues in terms of chemical properties and structure; 4. ACP has excellent biocompatibility and bioresorbability so that it can be used for manufacturing of artificial bone grafts [2]. Besides, ACP has various potential

applications such as drug carriers, vectors for delivery and release of viruses and DNA in transfection procedures as well as membranes for separation of large polymers [3]. With the help of templates, the structures of synthesized ACP nanomaterials can be controlled. Specifically, a variety of liquid crystalline phases (LCPs), possessing different phase structures such as lamellar, reverse hexagonal, normal hexagonal, cubic phases, etc, can be used as organic templates for CaP synthesis. As a result, CaPs with different structures such as sheets, rods, and mesoporous structures, etc. could be possibly replicated from the corresponding LC template.

1.3 Biomineralization

Biomineralization refers to controlled formation of minerals within living organisms. Fig.1 shows an example of this, displaying various polymorphs of calcium carbonate. Nowadays there are over 60 types of minerals that can be found in living organisms, for example, shell and teeth [1]. Quantity wise, CaPs account for a small fraction of all the biological minerals compared with silicon dioxide and calcium carbonate. It is of great interest to understand and mimic bone mineralization. Studies carried out by Sommerdijk and co-workers can provide an insight into the model systems of biomineralization [4, 5]. Nudelman et al. reported that ACP pre-nucleation clusters could infiltrate into collagen matrix and transform into oriented bone mineral in the presence of extra-fibrillar nucleation inhibitors [4]. In another study, Dey et al. reported the important role of pre-nucleation clusters played when CaP crystallization is induced on a surface [5].

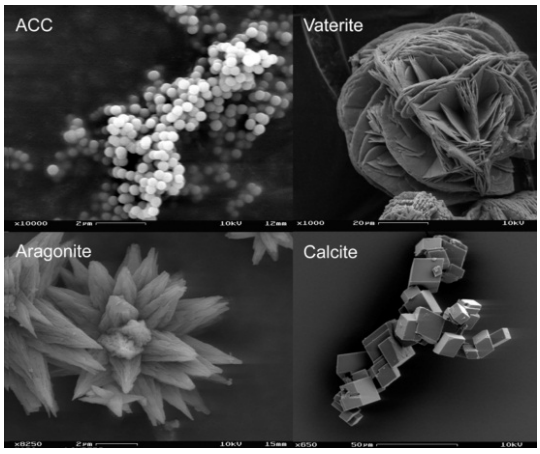

Figure 1: polymorphs of calcium carbonate: amorphous calcium carbonate (ACC), vaterite, aragonite and calcite.[6]

1.4 Project work

The current project aimed to control the morphological development of CaPs in

organic templates (i.e., surfactant self-assembled LCPs) and form CaPs with defined nano-structures. For a better understanding on bone mineralization, the knowledge of *in vitro* CaP morphogenesis in confined space is necessary. In this study, collagen matrix was simplified to LCPs, which were utilized as templates for the formation of CaPs. The experiment was carried out following the procedure:

1. Investigation of the formation of CaP nanomaterials using lamellar and reverse hexagonal LCPs as templates according to the ternary diagram of surfactant L64 (beaker method).
2. Investigation of the formation of CaP nanomaterials using cubic and normal hexagonal LCPs as templates according to the ternary diagram of surfactant F127 (beaker method and petri dish method).
3. Examination of the effects of reaction time, pH value, salt concentration and penetration rate of ammonia, etc. on CaP synthesis.
4. TEM and SEM Characterization and comparison of all the obtained CaP nanostructures when varying above mentioned conditions.

2 Theory

2.1 Bone mineralization [7, 8]

Bone is a kind of bioceramic composite in which nanoscale arrays of apatite are embedded within the gaps of collagen fibrils (as showed in Fig.2), meanwhile interacting with non-collagenous proteins (NCPs), resulting in a material, which is lightweight but extremely tough. There are many parameters influencing the physical and mechanical properties of bone, for instance, the size, shape and chemical composition of bone, as well as the spatial distribution and orientation of bone mineral within collagen fibrils, and so on. One characteristic of biomineralization is the strong interaction between inorganic phase and organic phase. Generally, the association between these two phases is at a superstructural level. At this level, mineral particles interact with biopolymers (collagen molecules for bone) and generate extremely strong and tough composites.

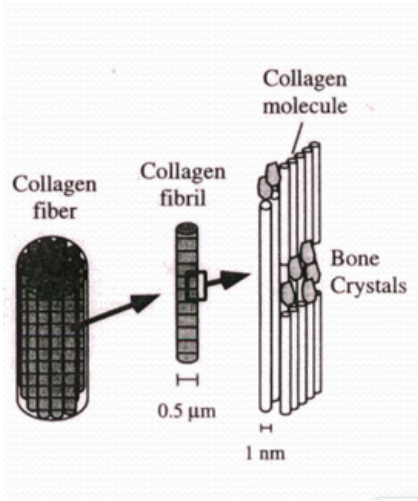

Figure 2: bone crystal embedded in the collagen matrix [11]

Many researchers have investigated the role of collagen and non-collagenous proteins on bone formation. Research carried out by Nudelman, et al. indicates that ACPs can transform into bone mineral in the presence of collagen and non-collagen proteins [4]. Specifically, in the presence of a protein called fetuin, ACPs are inhibited from crystallizing and will diffuse into collagen fibrils. Meanwhile, fetuin molecules stay just outside because they are too big to get access into the fibrils. Besides, the collagen actually triggers the oriented apatite nucleation without the interaction of NCPs. On the other hand, the NCPs themselves may not be able to be embedded into the fibril as a result of the high molecular weight. However, they could form a stable complex with CaP, allowing it to enter the collagen fibril [4, 9]. Fig.3 shows one possibility of how the bone mineral is formed from ACPs.

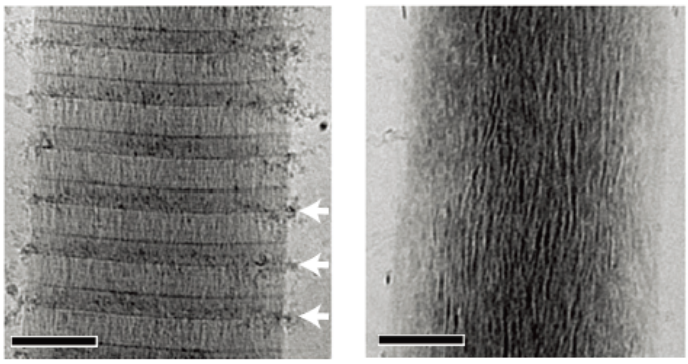

Figure 3: Mineral crystal (generated from ACP) embedded into the collagen fibrils. Scale bars: 100nm [9].

2.2 Inorganic morphogenesis [3]

Inorganic morphogenesis refers to the formation of inorganic materials with various structures. Learning inorganic morphogenesis can strengthen our understanding of biomineralization. The ordered pore network of zeolites is a typical example in terms of synthetic approaches to inorganic morphogenesis. Generally, the function of organic templates is to direct structures, reach charge balance and fill space. As-synthesized inorganic materials with complicated patterns have potential applications as new kinds of catalyst supports, biomedical implants, drug carriers as well as vectors for delivery and release of viruses and DNA in transfection procedures, membranes for separation of large polymers [3].

There are several kinds of inorganic morphogenesis. Firstly, transcriptive synthesis refers to that the patterns of inorganic materials can be replicated directly from pre-organized organic architecture. Secondly, synergistic synthesis emphasizes the co-assembly between inorganic and organic phases and these two components develop synergistically. Thirdly, metamorphic reconstruction describes that co-assembly takes place and new structures are formed, which differs from the initially designed co-assembly structures.

2.3.1 Transcriptive synthesis

In this synthesis method, the pattern of inorganic material resembles that of the organic template. The template is pre-organized, self-assembled and relatively stable. The structure of the inorganic material will transcript directly from organic template without the interaction between inorganic and organic phases. The CaP synthesized by the surfactant/water/oil LCPs are formed according to the transcriptive synthesis mechanism. The self-assembled surfactant templates will not interact with CaP precursor and as-prepared CaPs replicate the template structure directly.

2.3.2 Synergistic synthesis

In synergistic synthesis, interactions between inorganic and organic phases in the reaction system take place. A characteristic of this method is the co-adaptation of inorganic materials and organic templates. On the nanoscale, inorganic building blocks can be formed and co-assembled around organic molecules. Complementarily, chemical and structural properties of organic and inorganic counterparts on the interface determine how these two phases will be arranged.

2.3.3 Metamorphic reconstruction

New morphologies can be formed besides initial architecture due to changes in phase behavior, etc. This is triggered by initial growth and nucleation of an inorganic material in a multicomponent system, such as a surfactant/water/oil LCP. Some of the reconstructions might be confined to certain localized spots in the initial structure, while other relatively large changes could produce materials with complex structures that do not bear similarities to initial organization in the reaction system. Generally, it is believed that metamorphic reconstructions could take place during various stages of hierarchical synthesis of inorganic materials. Metamorphic reconstructions happen constantly during the inorganic/organic composite formation. If space cannot be efficiently filled as well as interfacial structures and charges are not matched, the inorganic/organic phase system can be very metastable, leading to deviation from the initial structure.

2.3 Liquid crystalline phases (LCP) [10]

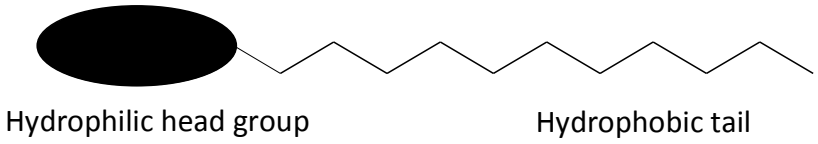

Figure 4: Scheme of a surfactant molecule

2.3.1 Driving forces of micelle formation

Fig.4 shows the structure of a surfactant molecule. Surfactants are amphiphilic. It contains at least two parts, namely hydrophobic tail and hydrophilic head group. When surfactants are added into water, the hydrophobic tail wants to minimize its contact with water and tend to be expelled from water phase. Therefore, it prefers to hide inside micelle (if the concentration is above the CMC) while the hydrophilic part inclines to interact with water. In addition, the repulsion between hydrophilic head groups keeps individual micelles from being aggregated. The repulsion force is strong

enough to prevent phase separation in the surfactant system. Therefore, the situation shown in Fig 5.a will occur. On the other hand, when surfactants are added into oil, an exact opposite scenario will happen, as illustrated in Fig 5.b. Note that there is a balance between hydrophobic and hydrophilic interactions, which determines whether micelles can be formed or phase separation would occur.

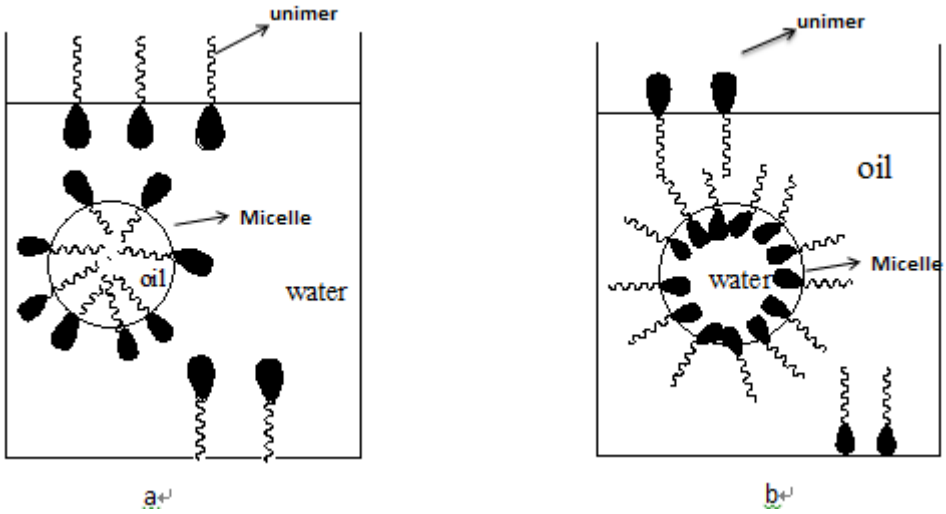

Figure 5: Micelle and reversed micelle formation of surfactants

2.3.2 Block polymeric surfactant

Block polymeric surfactants belong to the class of non-ionic surfactants, which is the second largest surfactant class. As for this kind of surfactants, hydrophobic and hydrophilic parts are similar in size and generally the hydrophilic part is larger than hydrophobic one. Block polymeric surfactants have a series of advantages [10], written as follows: 1: They are normally compatible with all other types of surfactants. 2: Contrary to ionic surfactants, their physicochemical properties are not markedly affected by electrolytes. 3: Block polymeric surfactants are more effective and can reach the same efficiency with lesser amount than ionic surfactants. 4: Block polymeric surfactants can be used to form inorganic materials with various structures and they are not sensitive to inorganic precursors. Fig.6 shows the ternary diagram of an amphiphilic block polymer/water/oil system and the various phases it can create.

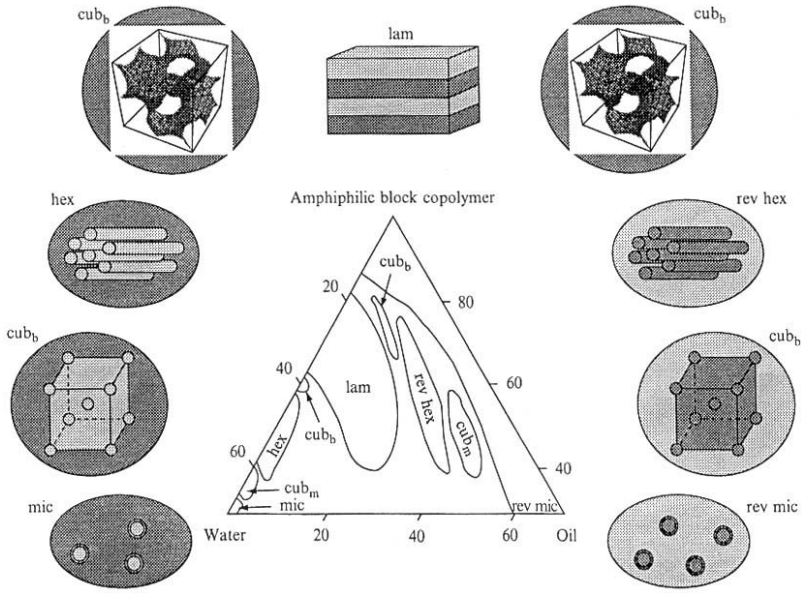

Figure 6: Ternary phase diagram of an amphiphilic block polymer/water/oil system and corresponding phase structures [10]

2.3.3 Ternary phase diagram

When surfactant is highly soluble in water, various phase structures can be formed with increasing surfactant concentration. Self-assembled LCPs with remarkable structures such as the lamellar phase (L_α), normal hexagonal phase (H_1), bicontinuous cubic phase (I_1), and reverse hexagonal phase (H_2), can be formed. According to phase diagrams, one knows what components that are needed and what phases that can be formed. In this project, ternary phase diagrams of two systems were utilized when forming the LCP templates. Generally we consider the phase behavior at a constant temperature. As for the ternary phase diagram in Fig.6, the information indicated is as follows: a collection of LCPs including cubic, reverse hexagonal, lamellar, normal hexagonal, reverse micelle and micelle phases can be obtained. At the same time, it can be noticed that a large range of block polymeric surfactant/ oil/water ratio can be utilized in order to form lamellar phase (as seen from the large area for lamellar structure, noted as "lam" on Fig. 6.)

The following are the LCPs utilized in the present study.

a. Normal hexagonal phase (H_1)

H_1 phase has water as continuous phase, which contains cylindrical domains that consist of oil. The phase is established by long cylindrical micelles, which form a hexagonal pattern and each micelle is surrounded by six other micelles. The radius of the micelle is close to the molecular length of the surfactant.

b. Lamellar phase (L_α)

As for this phase, bilayers formed by surfactant molecules alternate with water layers. The bilayer has a thickness less than twice the length of surfactant molecule. The thickness of water layer can be very different for different surfactants.

c. Bicontinuous cubic phase (I_1)

There is more than one structure for this phase, the surfactant form aggregates that present a porous three dimensional network; the structure can be considered to be formed either by connected rod like micelles or bilayer structures.

d. Reverse hexagonal phase(H_2)

Only L_α phase is symmetrical around the middle of the bilayer, other phases have a reversed counterpart in which the polar and non-polar parts have changed roles. H_2 phase is the reversed counterpart of H_1 phase and it is built up of hexagonally arranged water cylindrical domains in oil as continuous phase [10].

2.4 Amorphous solids versus crystalline solids [1]

It is impossible to find infinitely perfect crystals from a thermodynamic perspective. There are many kinds of disorders, for example, dislocations and grain boundaries in the common crystals. These disorders can disrupt the periodicity of crystals so that crystals will not be perfect. Meanwhile, they have some impact on the physical properties of these crystals. However, there also exist some solids which are extremely disordered so that we have to give up the concept of lattice which is an important characteristic of crystals. These highly disordered materials are called amorphous materials. Amorphous structures are largely distinct from densely packed crystals. In some cases, perfectly ordered structures cannot be compared from amorphous materials. We always use the shortest length scale of one atom with or without its neighbor of two or three atoms to describe the structure of an amorphous material. This kind of structures can always be found in all solids and liquids, which is called a short range order. For solids in crystalline state, ordered structure can be achieved with arrangements of tens or hundreds of atoms. These materials have a Long Range Order (LRO) and most metals belong to this category. Non-crystalline solids, for instance, glasses, do not have a LRO and are considered as amorphous solids even though they have a well-defined Short Range Order (SRO).

Many scientists have agreed on how to classify these orders of different levels. Regarding the distance between atoms in a solid, 0.2nm~0.5nm is categorized as SRO while 0.5nm~2nm is MRO with LRO referring to distance larger than 2nm. In order to examine the tiny structures of a solid, Transmission Electron Microscopy (TEM)

and Small Angle X-ray Scattering (SAXS) are utilized to detect the distinction of the crystalline and amorphous structures on LRO level.

2.5 Characterization

2.5.1 Transmission Electron Microscopy (TEM) [11]

TEM measurements provide lots of information, such as morphological and crystallographic information as well as the composition of samples. In a TEM, electrons travel through specimen and hence the image will be a 2D projection of a 3D object. The acceleration voltage of up to date routine instruments is 120 to 200 kV. The operating mechanism of TEM is on the same basic principles as that of light microscope but uses electrons instead of light. TEM has much higher resolution, which can be as high as 0.1 nm. The sample for TEM analysis needs to be very thin, about 100 nm thick or less, so that it is transparent for electrons. Absorption of electrons plays a minor role in image formation. Figure 7 shows a JEOL JEM-i200 EX TEM microscope, with the accelerating voltage up to 120 kv.

Figure 7: TEM: JEOL JEM-1200EX [12]

2.5.2 Scanning Electron Microscopy (SEM) [11]

SEM is a technique used to obtain topographic, morphological, compositional and sometimes, crystallographic information of an object at micro- and nanoscopic level. The magnification of SEM is between 12x-900Kx and the resolution can reach as high as 1.5 nm. When using SEM, a vacuum environment is required so that the path of primary beam through the electron optic column will not be hindered by the presence of other molecules. In the meantime, the ionization of gases will not occur. Higher acceleration voltage gives higher signal but is less surface sensitive. So in

general, we choose relatively low voltage to visualize the surface features. The SEM instrument we used (as Fig. 8 shows) was Leo Ultra 55 FEG SEM with the magnification from 12x-900kx.

Figure 8: Leo Ultra 55 FEG SEM [13]

3 Experiments

3.1 Materials

All chemicals were of analytical grade, purchased from Sigma-Aldrich and used without any further purification.

3.1.1 Calcium and phosphorus sources:

Calcium nitrate tetrahydrate [$Ca(NO_3)_2 \bullet 4H_2O$] and 85 wt% phosphoric acid (H_3PO_4) were the sources for the preparation of calcium phosphate.

3.2 LCP systems

Two types of Pluronic surfactants were selected for the formation of LCPs, namely Pluronic L64 ($EO_{13}PO_{30}EO_{13}$) and F127 ($EO_{100}PO_{70}EO_{100}$).

3.2.1 The ternary phase diagram of L64/p-xylene/H_2O system [11]

Pluronic L64 was used for the formation of lamellar (L_α) and reverse hexagonal (H_2) phases. The ternary diagram of Pluronic L64 ($EO_{13}PO_{30}EO_{13}$), is shown in Fig. 9, and consists of three components, which are L64, H_2O and p-xylene.

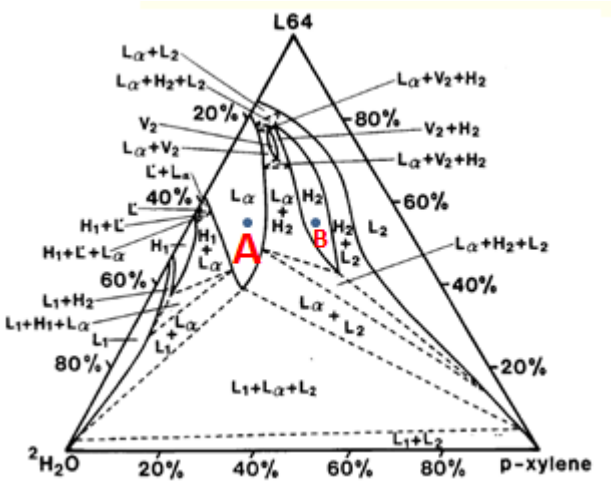

Figure 9: the ternary diagram of L64/p-xylene/H_2O system [14]

The recipe utilized for forming a H_2 phase was marked as dot B in Fig. 9, while that of L_α phase was noted as dot A. The specific weight percentages of the three components in each phase are listed in Table 2.

Table 2: Recipe for LCPs formed by L64

Phase structure	L64	p-xylene	aqueous solution
Reverse hexagonal (H_2)	70 wt%	15 wt%	15 wt%
Lamellar (L_α)	55 wt%	10 wt%	35 wt%

3.2.2 The ternary phase diagram of F127/butanol/H_2O system[15]

Pluronic F127 was used to form LCPs with cubic (I_1) and normal hexagonal (H_1)

structure. The ternary diagram of F127 ($EO_{100}PO_{70}EO_{100}$) (as shown in Fig. 10) consists of three components, which are F127, H_2O and Butanol.

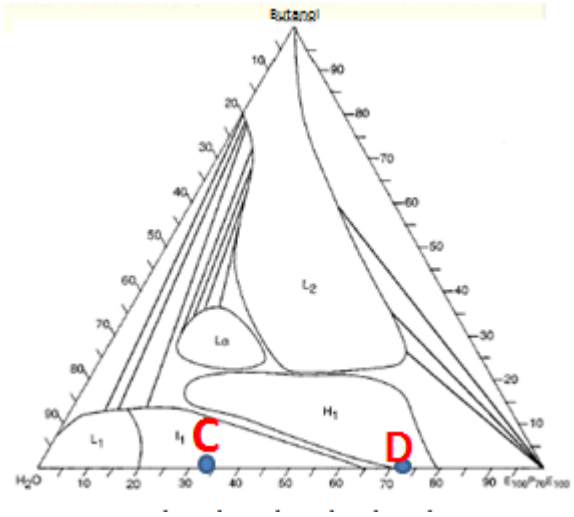

Figure 10: the ternary diagram of F127/butanol/H_2O system[15]

The recipe utilized for forming a hexagonal phase was 25 wt% aqueous solution, 75 wt% F127 marked as dot D in Fig. 10. Cubic phase with a composition of 65 wt% aqueous solution, 35 wt% F127 was also prepared as can be seen from the dot C in Fig. 10.

3.3 Synthesis [16,17]

$Ca(NO_3)_2 \bullet 4H_2O$ and H_3PO_4 with a Ca/P ratio of 1.67 were dissolved in Milli-Q water at different initial concentration: 20 wt%, 30 wt%, where the numbers were the weight percent of $Ca(NO_3)_2 \bullet 4H_2O$ in aqueous solution.

3.3.1 LCP route: beaker method

This method was employed for the preparation of LCPs with L_α and H_2 structures using surfactant L64 as well as I_1 and H_1 phases using Pluronic F127.

For the formation of LCPs, the prepared aqueous solution, Pluronic surfactant (L64 for L_α and H_2 phases and F127 for I_1 and H_1 phases) and oil (p-xylene for L64 system and butanol for F127 system) were evenly mixed.

Several glass vials (20 mL, 57.00×27.50 mm, VWR) were then filled with c.a. 15 g of as-prepared LCP gel and they were tightly sealed and left stored to reach equilibrium. In one of the glass vials, pH paper (pH range is 1~14) was cut into small pieces and mixed with LCP gel, which was later used as a pH indicator for the reaction. After being stored for 24 hours, the glass vials filled with gel were placed into a reaction box with ammonia atmosphere (ammonium hydroxide, 35 wt% ammonia, aqueous

solution) to initiate the reaction. After certain days, the glass vials were taken out from reaction box and gel samples were collected from at least two different layers with different pH ranges (pH value were read from the pH indicator, as shown in Fig. 11). The gel samples were dissolved in ethanol and centrifuged (Hettich ALC) at 2500 rpm for 10 min. Then the supernatant was removed gently and the sedimentation was re-dispersed in ethanol. This purification process was repeated for 3 times and the final dispersion was used for preparing TEM samples. Extra sample dispersion were stored in the fridge at 4 °C.

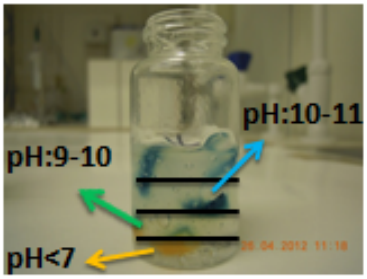

Figure 11: pH indicator after reaction

3.3.2 LCP route: petri dish method

This method was employed for the preparation of LCPs with I_1 and H_1 phases using Pluronic F127. Comparing to the "beaker method", "petri dish method" was different in two ways: 1. The LCP was formed by evaporation-induced self-assembly to achieve a thin flat gel layer of 1–2 mm thickness; 2. To slow down the release rate of ammonia, therefore to control the reaction speed in gel layer, ammonia was mixed with surfactant to form a LCP as well. Specifically:

1. For LCP gel preparation: as-prepared salt solution and F127 were evenly mixed according to the recipe listed in Table 3. Then ethanol (15g, 95 wt%) was added into LCP (50g) to reduce its viscosity. After that, c.a. 9.5 g of this mixture was poured into petri dish to form a thin film. The petri dish was left wide open for 30 minutes to let ethanol evaporate. Then it was covered by glass slide for further stabilization. After 24 hours, the petri dish with a thin flat layer of LCP gel was placed into a reaction box with ammonia atmosphere (ammonia solution mixed with F127) to initiate the reaction. After certain days, gel samples were collected and purified following the same process as described in "beaker method".

2. To prepare an ammonia-surfactant mixture, 25 wt% of ammonium hydroxide (35 wt% ammonia, aqueous solution) was mixed with 75 wt% of F127 and a H_1 phase was formed. A beaker containing ammonia mixture was placed at the bottom of reaction box, where the petri dish was placed on the top floor in the box (as shown in

Fig. 12).

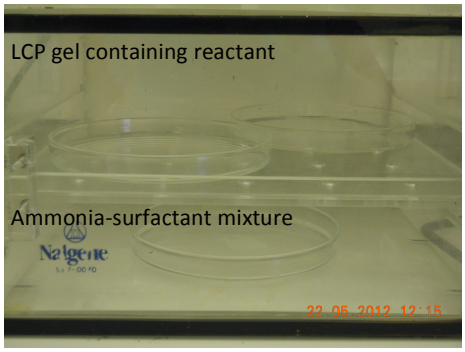

Figure 12: two petri dishes of LCP gel in ammonia atmosphere

3.4 Characterization of synthesized particles

For the as-prepared CaP particles, TEM and SEM were utilized to obtain microstructural information. Sample morphology was investigated by TEM, performed on a JEM-i200 EX microscope (JEOL Ltd.), operated at 120 kv. TEM specimens were prepared as soon as the collected gel had been purified and centrifuged. After dispersing particles in ethanol, the TEM sample was prepared by placing a drop of sample solution onto TEM grid and air-dried.

TEM samples were also taken to SEM characterization on a Leo Ultra 55 FEG SEM, operated at 5 kv.

4 Results and discussions

4.1 LCP gel formation

The formed H_2 LCP with a composition of 15 wt% salt solution, 70 wt% L64 and 15 wt% p-xylene were transparent, birefringent and highly viscous while the liquid crystal of L_α structure prepared by mixing 35 wt% salt solution, 55 wt% L64 and 10 wt% p-xylene were transparent, birefringent and had certain fluidity.

The formed H_1 LCP with a composition of 25 wt% salt solution, 75 wt% F127 were transparent, birefringent and highly viscous while the I_1 LCP prepared by mixing 65 wt% salt solution, 35 wt% F127 were transparent, non-birefringent and extremely viscous.

4.2 Particle formation process in LCPs

This part will be divided into four subparts and four kinds of phases, namely L_α, H_2, I_1 and H_1 phases will be discussed respectively.

4.2.1 L_α phases

The reaction between calcium and phosphorus precursors was triggered by the increase of pH in aqueous domain as a result of the gradual penetration of NH_3 into LCP gel. With time, the gel was no longer transparent, which indicated that solid particles had been formed inside the water domains. An apparent interface could be seen between the reacted and unreacted gel layer, as shown in Fig.13. It can be proposed that at different gel layers, the reaction proceeded at different stages. This phenomenon is understandable since the reaction stage of a specific gel layer was determined by its reaction time, i.e. longer time in ammonium. For instance, the reaction of a gel layer that is close to the air-gel interface would start earlier and progress longer and more rapidly than that of a gel layer that is close to the bottom of the same glass vial. Therefore, parameters like the distance from the air-gel interface as well as the penetration rate of ammonia can greatly affect the final product.

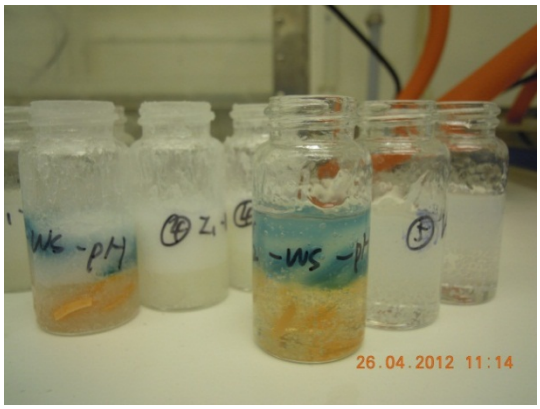

Figure 13: the opaque gel after reaction

The following four parameters were taken into consideration when synthesizing CaP in L_α phase.

1, Salt concentration

The initial concentration of calcium and phosphorus precursors in aqueous solution can influence the formation rate of CaPs to some extent. We investigated the difference between 20 wt% and 30 wt% as the initial salt concentration.

2, Reaction time in ammonium

Reaction time was measured by the number of days that glass vials remained in the ammonia atmosphere. Empirically, glass vials with L_α gel stayed in ammonia atmosphere for one or two days before sample collection and purification.

3, Penetration rate

Penetration rate was controlled by the amount of ammonia that was added into pH reservoir in the reaction box.

4, Distance from the air-gel interface

When the whole glass vial reactor was put into ammonia atmosphere, the gels at different layers had different reaction time, as there had been a pH gradient through the whole LCP gel (thickness: c.a. 45mm). It is also an important parameter for CaP synthesis.

With these parameters considered, the reacted L_α gels at certain layer were collected and the TEM images of resulted CaP particles are shown in Fig. 14.

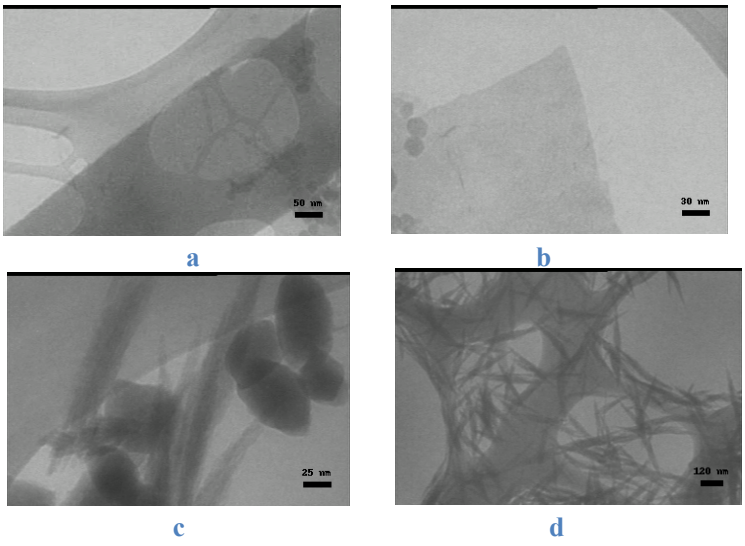

Figure 14: TEM images of CaPs prepared in L_α LCP with initial salt concentration of 30 wt% and reaction time of a. b 2 days and c. d 1 days. Scale bars: a. 50 nm, b. 30 nm, c. 60 nm, d. 120 nm.

As can be seen in Fig. 14 a and b, CaP particles with sheet-like morphology were successfully synthesized from L_α LCP template. These thin sheets presented a breadth

larger than 200 nm and thickness less than a few nanometers. Comparingly, Fig. 14 c, d present mostly crystalline CaPs with needle-like morphology as well as relatively large ACP spheres, which indicate that these syntheses were unsuccessful. In order to obtain sheets, the penetration time is a very important parameter, which contributes to the successful synthesis as well as the reaction time and pH value. It is hypothesized that the crystalline structure of CaP from the unsuccessful syntheses (Fig. 14 c, d) was due to the high penetration rate of ammonia, resulting the drastic increase of pH in upper layer. Therefore, the upper layer produced the crystalline structure and the further penetration of ammonia was blocked. Besides this, large ACP spheres were formed from unreacted gel during purification, as they reacted in relatively unrestricted environment in the presence of ammonia and surfactant while the gel was dissolved in ethanol.

4.2.2 H_2 phase

Many experiments were carried out for the synthesis of CaP using H_2 phase as template with varying conditions. Parameters such as reaction time, penetration rate, pH value and initial salt concentration were also examined as performed in the case of the syntheses using the L_α phase.

Fig. 15 shows the morphologies of synthesized CaP with initial salt concentration of 30 wt%. In this system, it seems that 5 days of reaction time is much better than 3 days in terms of producing rods, since rod-like CaP particles were dominant on day 5 (Fig. 15 b.1–3), while on day 3 (Fig. 15 a) 90 % of CaP particles were spherical.

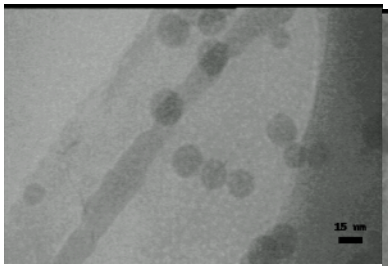

a

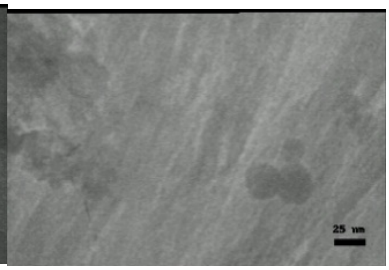

b.1

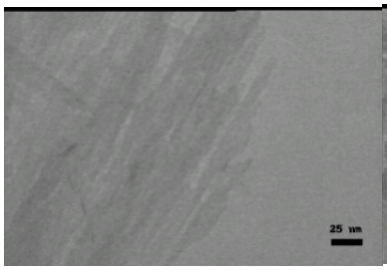

b.2

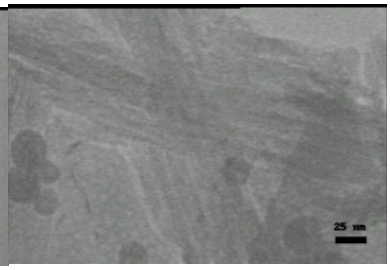

b.3

Figure 15: TEM images of CaPs prepared in H_2 LCP, with initial salt concentration of 30 wt% and reaction time of a. 3 days and b. 5 days. Scale bars: a. 15 nm, b.1–3 25 nm.

With reaction time longer than 3 days and well-controlled ammonia penetration rate, the experiments for forming CaP rods were proved to be reproducible.

The following images show the structure difference of synthesized CaPs with initial salt concentration of 20 wt%. By comparing Fig. 16 a and b. 1-4, it can be noticed that with well controlled ammonia penetration rate, reaction time of 4 days contributes to the sample with much more rods than that of 3 days. With reaction time longer than 3 days, there is a strong tendency for rods to be formed, as shown in Fig. 16. Fig. 16 b and d further certify that the longer time LC gel reacted in ammonia atmosphere, the more rod structure dominated in CaP samples. Furthermore, the comparison between Fig. 16 b, c and d, e seems to boil down to the conclusion that gel samples with pH 10-11 possess more rods than those collected at pH range of 9-10.

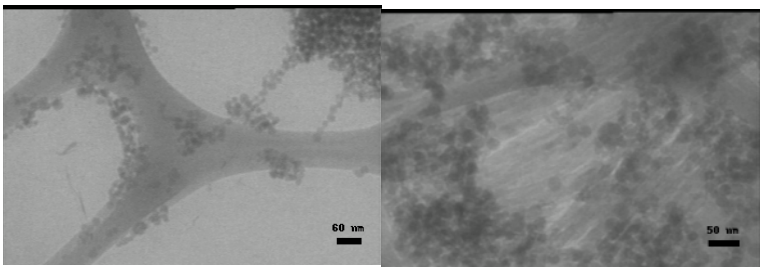

a b.1

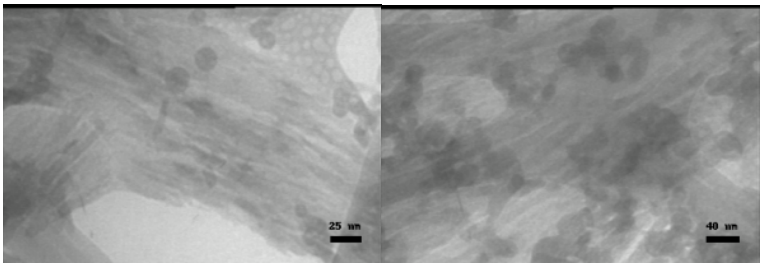

b.2 b.3

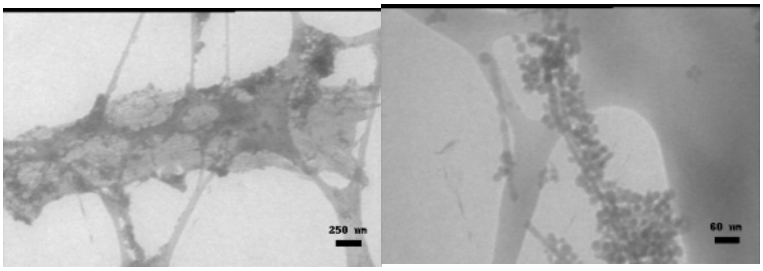

b.4 c

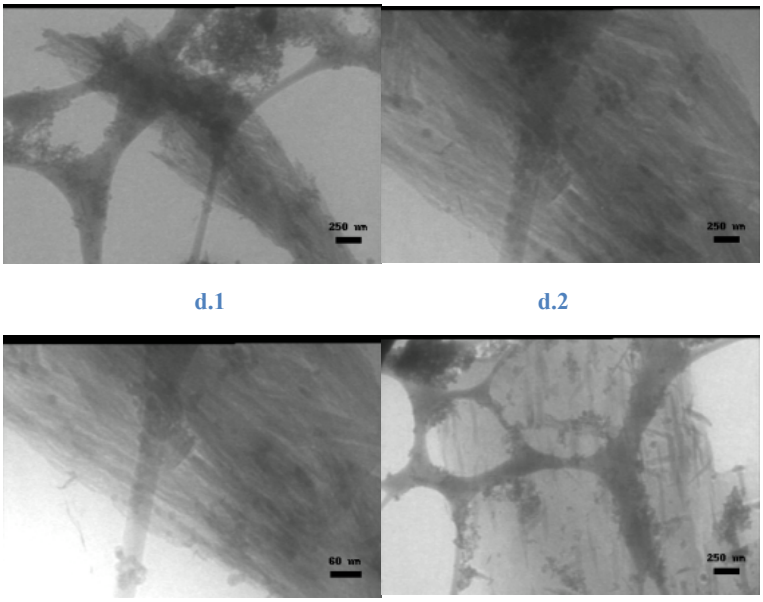

d.1 d.2

d.3 e

Figure 16: TEM images of CaPs prepared in H_2 LCP, with initial salt concentration of 20 wt% and reaction time of a. 3 days, b–c. 4 days and d–e. 5 days. Note that the samples were collected from gel layers with pH range of: a: 9-10; b.1–4, d.1–3 pH 10–11; c, e. pH 9–10. Scale bars: a, c, d.3 60 nm; b.1 50 nm; b.2 25nm; b.3 40nm; b.4, d.1, d.2, e. 250 nm.

Based on these results we can summarize the following:

If the penetration rate of ammonia can be well controlled, the longer time LCP reacted in ammonia atmosphere, the more likely it is get nanorods. If the ammonia penetration rate is too fast, i.e. pH increases too fast in the water domain in the gel, ACP particles with irregular shape and dimension or even hydroxyapatite (HA) crystals will be formed. This is because the template is self-assembled by surfactants, which are rather "soft" in terms of regulating CaP growth so that the CaPs will not be easily restrained in this confined soft structures. Instead, CaPs grow fast into crystalline structures when the ammonia release is not controlled. Therefore a moderate ammonia penetration speed is required for the controlled formation of CaP particles without breaking down the surfactant template structure.

4.2.3 H_1 phase and I_1 phase

As for petri dish method, the parameters controlled during synthesis were reaction time and initial salt concentration. Since ammonia penetration was slowed down by using an ammonia release system of H_1 LC phase (ammonia-F127 mixture), as well as that the reactant-containing gel was a thin film, gel samples were considered as having little pH gradient and harvested as a whole layer. As follows are the TEM pictures obtained from the petri dish method. As can be seen from Fig.17, with a reaction time of 2 days, flakes with micrometer sizes (Fig. 17 d, e) as well as

aggregates of nano-filaments (Fig. 17 f) were formed from I_1 LC phase. While with a reaction time of 3 days, nanoparticle aggregates (Fig. 17 a, b) and thin flakes (Fig. 17 c) were formed from H_1 LC gel. These results reflect the complexity of CaP formation process. However, further investigations are needed to clearly understand the mechanism of CaP morphological control by LC phases.

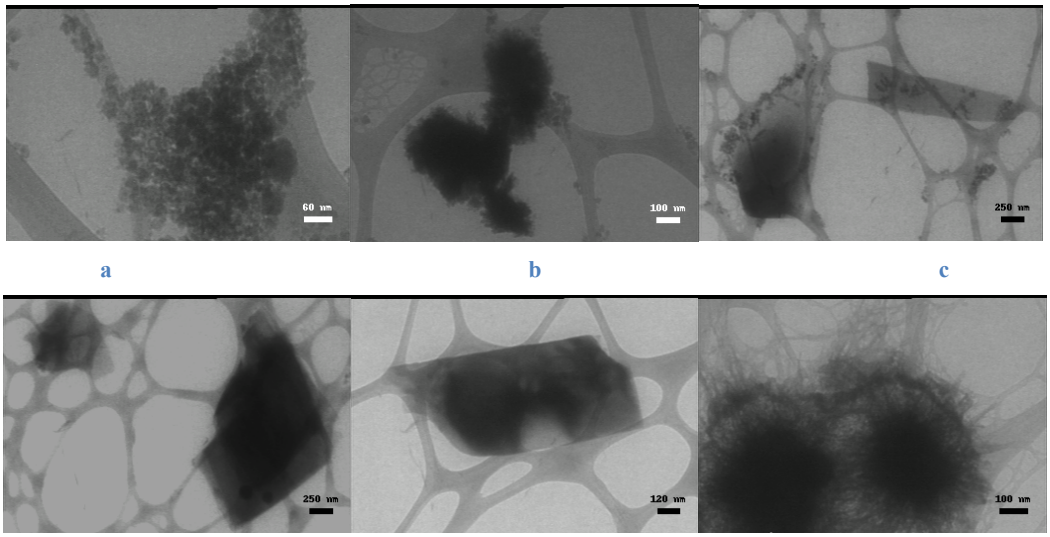

a b c

d e f

Figure 17: TEM images of CaPs prepared in H_1 LCP (a-c) and I_1 LCP (d-f). with initial salt concentration of 20 wt% and reaction time of a-c. 3 days, d–f. 2 days. Scale bars: a. 60 nm, b. f, 100 nm, c. d, 250 nm, and e.120nm.

As for beaker method, the parameters of reaction time, ammonia penetration rate, pH value and initial salt concentration were examined as performed also in case of the L_α phase and H_2 phases. Following are TEM images of the samples prepared from H_1 and I_1 phases. Instead of showing apparent mesoporous structures (alternating black and white stripes in TEM images), we gained some interesting structures as you can see from Fig. 18.

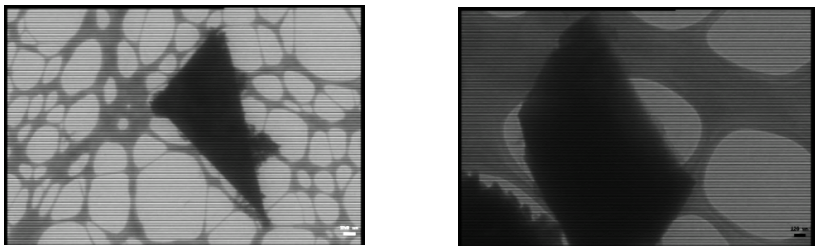

a b

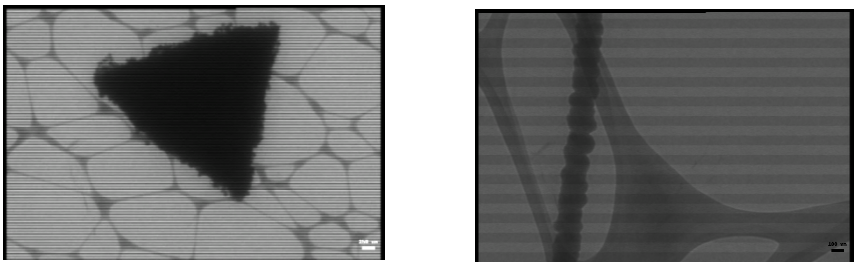

c d

Figure 18: TEM images of CaPs prepared in H_1 (a, b, c) and I_1 (d) LCPs, with initial salt concentration of 20 wt% and reaction time of 3 days. Note that the samples were collected from gel layers with pH range of 9-10. Scale bars: a. 120 nm, b, d. 250 nm and c. 100 nm.

However, it is difficult to detect whether these particles are mesoporous or not. It can be seen from the images that these structures are very thick. In order to visualize the structures more clearly, samples need to be subjected to higher electron dose, which in turn deteriorates the sample due to electron beam damage.

SEM measurements were also performed to examine the topological features of as-prepared particles, as shown in Fig. 19. It can be seen clearly that there exists facets in many particles. Fig 19 a.1 and a.2 show the same faceted particle subjected to electron beam with different time length. A severe deformation on the particle surface can be observed in Fig 19 a.2 with longer electron beam exposure time, which shows the difficulty of looking into detailed structure of the faceted CaP samples.

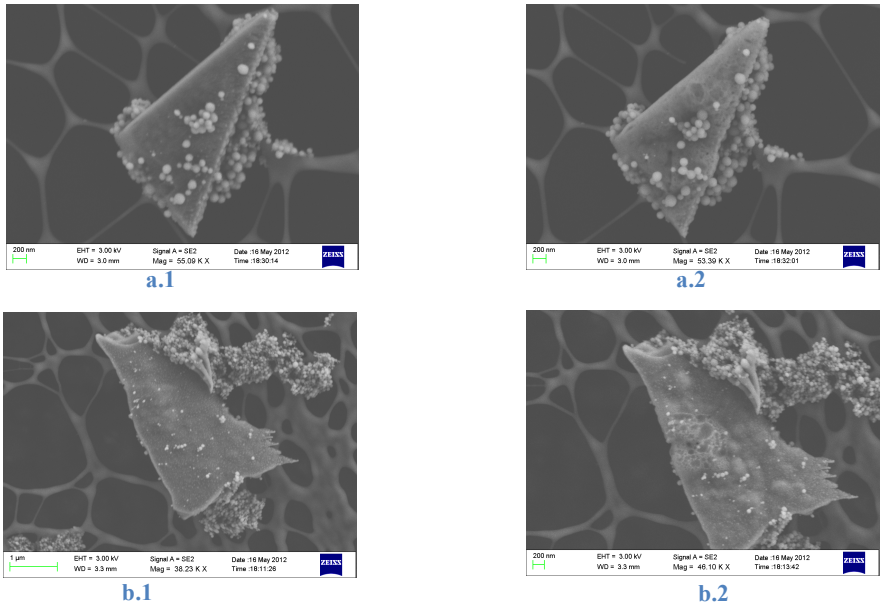

a.1 a.2

b.1 b.2

Figure 19: SEM images of the faceted CaP particles prepared in H_1 LCP. with initial salt concentration of 20 wt% and reaction time of 3 days. Note that the samples were collected from gel layers with pH range of 9-10. Scale bars: a.1, a.2 and b.2 200 nm, b.1 1 µm.

5 Conclusions

1. It is feasible and promising to synthesize calcium phosphates with different structures using self-assembled surfactant templates. However the obtained CaPs with designed structures are not stable as they are prone to convert to crystalline apatite. Therefore, it is important to harvest the material "in time" to prevent further crystallization of CaPs.
2. CaP morphogenesis is a complicated process that is governed by many factors: reaction time, salt concentration, reaction rate (affected by the NH_3 penetration speed), pH value and so on. Relatively slow penetration of ammonium (slow reaction rate) seems good for the formation of desired structures.
3. H_2 phase (with 15 wt% H_2O domain) is a better template then L_α (35 wt% H_2O domain), H_1 and I_1 phases.

6 Future work

1. Try to synthesize sheets using petri dish method.
2. Investigate more into the structures with facets.

7 References

1. Sergey V, et al. Amorphous calcium (ortho) phosphate. Acta biomaterialia. 2010, 6: 4457-4475.

2. Sergey V. Dorozhkin, et al. Biological and medical significance of calcium phosphates. Angewandte Chemie International Edition.2002, 41: 3130-3146.

3. Stephen Mann, et al. Synthesis of inorganic materials with complex form. Nature, 1996, 382: 313-318

4. Fabio Nudelman, et al. The role of collagen in bone apatite formation in the presence of hydroxyapatite nucleation inhibitors. Nature materials, 2000, 9: 1004-1009.Liam C. Palmer, et al. Biomimetic systems for hydroxyapatite mineralization inspired by bone and enamel. Chemistry review.2008, 108(11): 4754-4783.

5. Archan Dey, et al. The role of prenucleation clusters in surface induced calcium phosphate crystallization. Nature materials, 2010, 9: 1010-1014.

6. http://www.ruhr-uni-bochum.de/sediment/forschung.html.

7. Matthew J. Olszta, et al. Bone structure and formation: a new perspective. Material science and engineering. 2007, 58: 77-116.

8. Stephen Mann. Biomineralization: the hard part of bioorganic chemistry. Journal of Chemical Society Dalton Transactions. 1993, 1: 1-9.

9. Zhang Xu, et al. A biomimetic strategy to form calcium phosphate crystals on type I collagen substrate. Materials Science and Engineering. 2010, 30: 822–826.

10. Krister Holmberg, et al(2002). Surfactants and polymers in aqueous solution.Sweden, Umea: John Wiley & Sons.

11. Ludovico Cademartiri, et al (2010). Concepts of Nanochemistry. Germany, Weinheim: Wiley-VCH.

12. http://www-ne.mech.eng.osaka-u.ac.jp/Nakayamalab/english/tem1200_e.html

13. http://www.fy.chalmers.se/microscopy/instrumentation/SEM/Ultra.xml

14. Paschalis Alexandridis, et al. Self-Assembly of Amphiphilic Block Copolymers: The (E0)13(P0)30(E0)13-Water-p-Xylene System. Macromolecules. 1995, 28: 7700-7710.

15. Peter Holmqvist, et al. Phase behavior and structure of ternary amphiphilic block copolymer-alkanol-water systems: comparison of poly(ethylene oxide)/poly(propylene oxide) to poly(ethylene oxide)/poly(tetrahydrofuran) copolymers. Langmuir.1997, 13:247-2479.

16. Kjellin P, et al. Synthetic nano-sized crystalline calcium phosphate and method of production. International Patent No. WO 2005/123579 A1, 2005.
17. He WX, et al. Formation of Bone-like Nanocrystalline Apatite Using Self-Assembled Liquid Crystals. Chemistry Materials 2012, 24: 892-902.
18. Donglin Li, et al. Design and synthesis of self-ordered mesoporous nanocomposite through controlled in-situ crystallization. Nature Materials.2004, 3: 65-72.
19. Emilie M.Pouget, et al. The development of morphology and structure in hexagonal vaterite. Journal of the American Chemistry. 2010, 132: 11560-11565.
20. http://en.wikipedia.org/wiki/Vaterite.
21. http://en.wikipedia.org/wiki/Aragonite.
22. Julia Mahamid, et al. Amorphous calcium phosphate is a major component of the forming fin bones of zebrafish: Indications for an amorphous precursor phase. Editorial Board. 2008, 105(35): 12748-12753.
23. Sergey V. Dorozhkin. Bioceramics of calcium orthophosphates. Biomaterials. 2010, 31: 1465-1485.
24. Sergey V. Dorozhkin. Calcium orthophosphate cements for biomedical application. Journal of Material Science. 2008, 43: 3028–3057.
25. Hong Li. Collagen modulating crystallization of apatite in a biomimetic gel system. Ceramics International. 2011.37:2305-2310.
26. Yan Liu, et al. Hierarchical and non-hierarchical mineralisation of collagen. Biomaterials. 2011, 32: 1291-1300.
27. Christian Burger, et al. Lateral Packing of Mineral Crystals in Bone Collagen Fibrils. Biophysical Journal. 2008, 95: 1985-1992.
28. Xiaoke Li, et al. Preparation of bone-like apatite-collagen nanocomposites by a biomimetic process with phosphorylated collagen. Journal of Biomedical Materials.2007, 8: 293-300.
29. Celso A, et al. Synthesis of Calcium Phosphate Nanoparticles in Collagen Medium. Macromolecule. 2007, 253, 77–81.
30. Douglas D. Archibald, et al. Template mineralization of self-assembled anisotropic lipid microstructures. Nature. 1993, 364: 430-433.
31. Galo J. de A. A.Soler-lllia, et al. Chemical strategies to design textured materials: from Mircoporous and Mesoporous Oxides to nanonetworks and hierarchical structures. Chemical Review.2002, 102: 4093-4138.

32. Nobuaki Ikawa, et al. Unique surface property of surfactant assisted mesoporous calcium phosphate. Microporous and mesoporous materials. 2011, 141: 56-60.
33. Donglin Li, et al. Design and synthesis of self ordered mesoporous nanocomposite through controlled in situ crystallization. Nature Materials. 2004, 3: 65-72.
34. Paul Calvert, et al. The negative side of crystal growth. Nature. 1997, 386: 127-129.
35. Dominic Walsh, et al. Fabrication of hollow porous shells of calcium carbonate from self organizing media. Nature. 1995, 377: 320-323.
36. Daniel Hagmeyer, et al. Self assembly of calcium phosphate nanoparticles into hollow spheres induced by dissolved amino acids. Journal of materials chemistry. 2011, 21: 9219-9223.
37. Dominic Walsh, et al. Crystal tectonics: construction of reticulated calcium phosphate frameworks in biocontinuous reverse microemulsions. Science, 1994, 264: 1576-1578.
38. George S, et al. Liquid crystalline phases as templates for the synthesis of mesoporous silica. Nature.1995, 378: 366-368.
39. Daniela C.Popescu, et al. Template adaptability is key in the oriented crystallization of CaCO3. Journal of Chemistry Society. 2007, 129: 14058-14067.
40. Nobuaki Ikawa, et al. Templating Route for mesostructured calcium phosphates with carboxylic acid and amine type surfactants. Langmuir. 2008, 24: 13113-13120.
41. Stephanie M. Schmidt, et al. Surfactant based assembly of mesoporous patterned calcium phosphate micron sized rods. Microporous and mesoporous materials. 2006, 94: 330-338.
42. Chao Liu, et al. Template synthesis and characterization of highly ordered lamellar hydroxyappatite. Applied surface science. 2007, 253: 6840-6843.
43. Jong Seto, et al. Structure-property relationships of a biological mesocrystal in the adult sea urchin spine. Editorial Board. 2012, 109: 3699-3704.
44. Emile Pouget, et al. Hierarchical architectures by synergy between dynamical template self-assembly and biomineralization. Nature Materials.2007, 6: 434-439.
45. Daniel Hagmeyer, et al. Self-assembly of calcium phosphate nanoparticles into hollow spheres induced by dissolved amino acids. Journal of Materials Chemistry. 2011, 21: 9219-9223.

46. Archan Dey, et al. In situ techniques in biomimetic mineralization studies of calcium carbonate. Chemical Society Reviews.2010, 39, 2: 397-409.
47. Rui-Qi Song, et al. Mesocrystal-ordered nanoparticle superstructures. Advance materials. 2010, 22: 1301-1330.

8 Acknowledgements

- Krister Holmberg for being my examiner and your guidance through the whole year.
- My professor, Martin Andersson for my opportunity to work on this interesting project and

your inspiration in every group meeting.

- My supervisor Wenxiao He for guiding me through the whole project.
- All the people in our group Maria Claesson, Johan Karlsson, Emma Westas for nice group collaboration.
- As well as at the whole applied surface chemistry department: Kurt Löfgren, Ann Jakobsson, Fengfeng Ding, Ye Li, Ning Yuan, Oskar ……
- My dear friend Wenjun Sun, Nan Wang.